Plankton cells in turmoil and the dynamics of heavy impurities with finite size

Lecture given on 30 June 2010 by A. Provenzale

1 Introduction

In this lecture we shall focus on the dynamics of individual phytoplankton cells and on simple models to describe their motion in the fluid flow. Phytoplankton cells are small, with dimensions up to a few hundred microns. Individual phytoplankton cells immersed in water are advected by the surrounding flow, even though some species can resist passive advection by various means, such as varying their buoyancy and/or swimming. In addition, most plankton cells are slightly heavier than water and are thus subject to gravitational sinking (i.e., they are negatively buoyant).

If we want to describe the dynamics of a phytoplankton cell advected by a flow, we need to write the equations of motion for the cell. However, real phytoplankton cells usually have a very complex shape (which can change with time), are non-homogeneous in their interior, can vary their buoyancy and can emit substances that change the local fluid viscosity. In addition, they swim, grow, reproduce (split), and eventually die or are eaten by zooplankton (small, usually multicellular organisms which feed on algae). For fluffy bodies with spines, tails and flagella and an active life such as phytoplankters, the equations of motion are rather complicated, and one should resolve the Navier-Stokes equations with the correct boundary conditions on the mobile surface of the little plankter.

In this lecture we follow a traditional path for the GFD school, and simplify - even grossly oversimplify - the problem, by considering the dynamics of infinitesimally small, spherical heavy particles, with fixed shape and density, which are passively advected by a surrounding fluid flow, and we call them "impurities." Of course, our impurities are but a far image of phytoplankton cells in the ocean.

2 Plankton and turbulence: a matter of size

Most fluid flows in the ocean and in lakes are turbulent, especially in the upper mixed layer where phytoplankton thrive. Thus, on large scales, the world in which plankton cells live is a turbulent environment. However, individual cells are small, usually smaller than the Kolmogorov scale - the length scale which marks the transition from laminar flow at smaller scales to turbulent dynamics at larger scales. For this reason, individual phytoplankters experience a viscous, laminar and non-turbulent flow in their immediate surroundings.

The motion of sea or lake water under "normal" conditions (ignoring compressibility, thermodynamics, phase transitions and other complications) can be described by the incompressible Navier-Stokes equations,

$$\rho \frac{D\mathbf{u}}{Dt} = -\nabla p + \mu \nabla^2 \mathbf{u} - \rho g \hat{\mathbf{z}} + \mathbf{F} \tag{1}$$

where $\mathbf{u}(\mathbf{x}, t)$ is the fluid velocity, $\mathbf{x}$ is the spatial coordinate, t is time, ρ is the fluid density, p is pressure, μ is the dynamic viscosity, g is the gravitational acceleration, $\hat{\mathbf{z}}$ is the unit vector in the z direction, $\mathbf{F}$ is a generic body force (if present) and the substantial (or Lagrangian) derivative can be expressed as $D\mathbf{u}/Dt = \partial \mathbf{u}/\partial t + \mathbf{u} \cdot \nabla \mathbf{u}$. We have fixed the z coordinate to point vertically upwards. If ρ is assumed to be constant, the gravitation term can be absorbed in the definition of pressure.

Equation (1) is complemented by the incompressible version of the continuity equation,

$$\nabla \cdot \mathbf{u} = 0 \ , \tag{2}$$

and in this way we get a complete description of the fluid flow, four equations in four variables. Of course, to (try to) solve the equations we also need boundary and initial conditions.

The Reynolds number can be defined as the ratio between the strength of the nonlinear term, $\rho|\mathbf{u} \cdot \nabla \mathbf{u}|$, and that of the viscous term, $|\mu \nabla^2 \mathbf{u}|$. If we call U and L the typical scale of velocity and length, and scale time by L/U, we get that the Reynolds number is Re=UL/ν where $\nu = \mu/\rho$ is the kinematic viscosity. When the Reynolds number is smaller than one, i.e., the velocity and/or the length scale are sufficiently small, the flow is laminar and viscosity dominates. For Re$\rightarrow 0$, we can discard the inertial term in the Navier-Stokes equations and find viscosity-dominated special solutions. When Re$\gg 1$, the flow becomes turbulent and the fluid velocity varies intermittently and erratically in time and space, spanning a wide range of values.

The simplified form of the Navier Stokes equations given by eq.(1,2) with constant density describes the cleanest case of turbulence, i.e., homogeneous and isotropic three-dimensional turbulence. Physically, this type of flow is a good model for turbulence for scales up to a few meters, a reasonably-sized portion of the world for a phytoplankton cell.

To quantitatively describe this type of turbulence, we assume that the energy input in the flow takes place at a certain macro length scale, l_0, and dissipation takes place mainly at a very small scale, say l_D. In the scale range between l_0 and l_D, energy gets transferred to smaller and smaller length scales by the breakdown of the larger eddies into smaller ones. Here, an "eddy" is a generic, usually short-lived, vortical structure in the three-dimensional turbulent flow, and it is characterized by a given (approximate) length scale. If $l_0 \gg l_D$ and no forcing is present between these two scales, then we see the emergence of an inertial range where the dynamics is independent of dissipation and forcing. Assuming that the spectral energy transfer rate is constant in the inertial range, so to obtain a statistically stationary energy spectrum, and using simple scaling arguments, one can derive the form of

the energy spectrum in the inertial range, $E(k)$, which obeys the celebrated Kolmogorov's -5/3 law,

$$E(k) \sim \varepsilon^{2/3} k^{-5/3} \tag{3}$$

where k is the wavenumber (i.e., $2\pi/\lambda$ where λ is the wavelength) and ε is the energy dissipation rate per unit volume.

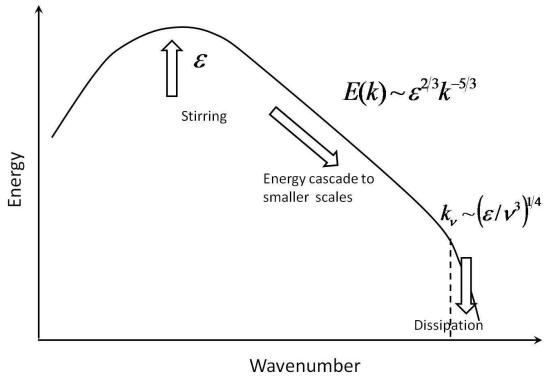

Figure 1: Energy spectrum of a three-dimensional, homogeneous and isotropic turbulent flow.

The length scale at which diffusion becomes important is called the Kolmogorov scale, l_ν, defined as

$$l_\nu \sim k_\nu^{-1} \sim (\nu^3/\varepsilon)^{1/4} \ . \tag{4}$$

At scales smaller than l_ν, the flow is laminar (but possibly unsteady). In the ocean, l_ν ranges between 6×10^{-5} m and 0.01 m. Since most phytoplankton cells are smaller than a few tens of microns in size, they do not experience a turbulent flow but are rather exposed to a viscous laminar flow.

The dominance of viscosity makes nutrient uptake by phytoplankton to be severely limited by molecular diffusion. For a plankton cell, nutrient delivery happens in two stages - nutrient delivery to the cell membrane and transport across the membrane. When the latter process is faster than the first one (as often happens), the nutrient concentration at the cell surface drops significantly below its far-field value. For a molecular diffusivity D and a plankton cell of radius a, the concentration of nutrient in the proximity of the cell wall is governed by the equation

$$\frac{\partial N}{\partial t} = D\nabla^2 N \tag{5}$$

whose spherically symmetric, steady state solution is

$$N(r) = \frac{a}{r}(N_0 - N_\infty) + N_\infty \tag{6}$$

where N_0 is the concentration at the cell surface and N_∞ is the far-field concentration. The diffusional flux to a spherical cell is then computed as

$$Q_D = 4\pi D a (N_\infty - N_0) \ . \tag{7}$$

When the uptake capacity of the cell exceeds the rate of nutrient supply by diffusion, a nutrient-depleted layer is formed near the cell. The time taken by diffusion for transporting the nutrient across this layer can be estimated as

$$T_D = \frac{a^2}{D} \ . \tag{8}$$

In water at standard upper ocean temperatures, for immotile cells with $a \leq 10\mu m$ the nutrient limitation can be severe.

Given that diffusion is not sufficient to bring enough nutrients to the cell surface, especially for smaller organisms, phytoplankters have found ways to overcome diffusion limitation. Most of these strategies are based on the ability of phytoplankters to move along trajectories which are not fluid particle paths, thus allowing them to explore new regions of the fluid which are not nutrient depleted yet. The differences between cell trajectories and fluid parcel trajectories can be generated, for example, by

1. Swimming (as many flagellates do);
2. Sinking (as diatoms do);
3. Exploiting the fact that plankton cells have different density from the fluid and have finite size.

In the rest of this Lecture, we shall focus on the last mechanism and study how heavy impurities with finite size (our gross model for plankters) are advected by a fluid flow.

3 Lagrangian advection

The motion of an advected particle with the same density of the fluid and vanishingly small dimensions (i.e., a fluid parcel) is described by the standard Lagrangian equations

$$\frac{d\mathbf{X}}{dt} = \mathbf{u}(\mathbf{X}, t) \tag{9}$$

where $\mathbf{X}$ is the particle position at time t and $\mathbf{u}(\mathbf{X}, t)$ is the fluid velocity at the particle position. Notice that equation (9) is non-Newtonian, in the sense that it does not obey the standard Newton's second law of motion. The reason is that the particle has no inertia with respect to the fluid, and thus we equate the Lagrangian particle velocity $d\mathbf{X}/dt$ to the Eulerian velocity $\mathbf{u}(\mathbf{X}, t)$.

Impurities with finite size and finite inertia do not behave like fluid particles. An impurity with density ρ_p moving with velocity $\mathbf{V} \equiv d\mathbf{X}/dt$ in a flow field $\mathbf{u}$ of a fluid with density ρ_f experiences forces due to gravity, $\mathbf{F}_g$, Stokes drag, $\mathbf{F}_s$, and the effect of the surrounding fluid (mainly pressure), $\mathbf{F}_f$, expressed as

$$\mathbf{F}_g = -g(\rho_p - \rho_f)\hat{\mathbf{z}}, \quad \mathbf{F}_s = -\frac{1}{\frac{4}{3}\pi a^3} 6\pi\rho_f \nu a(\mathbf{V} - \mathbf{u}) = -\frac{9\nu\rho_f}{2a^2}(\mathbf{V} - \mathbf{u}), \quad \mathbf{F}_f = \rho_f \frac{D\mathbf{u}}{Dt} \tag{10}$$

where, as before, a is the radius of the impurity.

Thus, using Newton's second law equating force to mass times acceleration, we can write for the motion of the impurity

$$\rho_p \frac{d\mathbf{V}}{dt} = \mathbf{F}_f + \mathbf{F}_s + \mathbf{F}_g \ . \tag{11}$$

Rewriting equation (11) we have

$$\frac{d\mathbf{V}}{dt} = \delta \frac{D\mathbf{u}}{Dt} - \frac{1}{\tau_a}(\mathbf{V} - \mathbf{u}) - (1-\delta) g\hat{\mathbf{z}} \tag{12}$$

where $\delta = \rho_f/\rho_p$ and $\tau_a = 2a^2/(9\delta\nu)$. The time scale τ_a measures the relaxation time of the particle velocity to the local fluid velocity and δ determines the nature of the buoyant particle ($\delta < 1$ and $\delta > 1$ indicate particles which are heavier or lighter than the fluid respectively).

In still fluid, where $\mathbf{u} = 0$, one can define the (downward) terminal velocity of the heavy impurity as

$$W = \frac{2}{9} g a^2 \frac{\rho_p - \rho_f}{\rho_f \nu} \ . \tag{13}$$

For example, an impurity with $\delta = 0.97$ and $a = 30\mu$m, as appropriate for a plankton cell, the terminal velocity W is a few meters per day.

It is important to stress the difference between the two time derivatives present in equation (14). While $D/Dt = \partial/\partial t + \mathbf{u} \cdot \nabla$ measures the rate of change along the path that a fluid particle would follow locally, $d/dt = \partial/\partial t + \mathbf{V} \cdot \nabla$ denotes the time derivative while tagging along the heavy impurity.

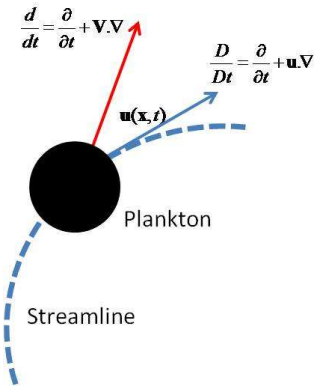

Figure 2: A graphical representation of the meanings of d/dt and D/Dt

Before proceeding further, we make eq.(12) non dimensional and write

$$\frac{d\tilde{\mathbf{V}}}{d\tilde{t}} = \delta \frac{D\tilde{\mathbf{u}}}{D\tilde{t}} - \frac{1}{St}(\tilde{\mathbf{V}} - \tilde{u}) - (1-\delta)\frac{1}{Fr^2}\hat{\mathbf{z}} \tag{14}$$

where the tilde is used to denote dimensionless variables. In the non-dimensional equation, $St = \tau_a U/L$ and $Fr = U/\sqrt{gL}$ are the Stokes and Froude numbers respectively and L and U are typical length and velocity scales. The Stokes number St represents the ratio between the particle relaxation time scale, τ_a, and the dynamical time scale L/U, whereas Fr quantifies the ratio of the buoyancy time scale, $1/\sqrt{g/L}$, to the dynamical time scale. In the following we will drop the tilde and denote the non-dimensional variables by the same notation as the dimensional ones, unless a distinction needs to be made.

4 Impurity advection in 2D stationary flows

In this section we study the dynamics of an ensemble of passive impurities advected by a stationary, divergence-free, two-dimensional (2D) cellular velocity field without the effects of gravity (we can think of a flow field on a horizontal plane). This example allows for stressing the differences between the dynamics of fluid parcels and that of heavy and light impurities; note that in this simple case one can rescale the Stokes number by rescaling time.

We first consider the case of an isotropic streamfunction $\psi = 2(\cos x + \cos y)$. The fluid velocity is $\mathbf{u} = (u, v)$ and the velocity components are given by $u = -\partial\psi/\partial y$ and $v = \partial\psi/\partial x$. In a 2D flow, fluid parcels obey the equations

$$\frac{dX}{dt} = -\frac{\partial\psi}{\partial Y} \ , \ \frac{dY}{dt} = \frac{\partial\psi}{\partial X} \tag{15}$$

which is formally an Hamiltonian system with phase space (x, y) where x and y are canonically conjugate variables and the stream function plays the role of the Hamiltonian. In this case, one has conservation of phase-space area and no preferential fluid particle concentration is possible. For a stationary flow, fluid parcels follow the streamlines; since the system is two-dimensional, there is no chaotic dynamics and the fluid parcels undergo only regular trajectories.

The situation is different for passive impurities, for which the phase space (x, y, V_x, V_y) is four-dimensional and the dynamics is dissipative. In the case of particles lighter than the fluid, $\delta > 1$, linear stability calculations show that the fixed points in $(x_n, y_m) = (2n\pi, 2m\pi)$ and $(x'_n, y'_m) = ((2n+1)\pi, (2m+1)\pi)$ (n, m being integers) are stable and attracting, while the fixed points $(\tilde{x}_n, \tilde{y}_m) = (2n\pi, (2m+1)\pi)$ and $(\tilde{x}'_n, \tilde{y}'_m) = ((2n+1)\pi, 2m\pi)$ are saddles. For heavy particles ($\delta < 1$), all these fixed points are unstable. In this case, the impurities undergo chaotic trajectories, hopping from one flow cell to another, and display non-turbulent diffusion, even in the case of a stationary velocity field [3].

Figure 4 shows how an initially homogeneous distribution of heavy and light impurities evolves in the prescribed flow. The short-time dynamics is very similar for both light and heavy particles. An interesting feature is the transformation of an initially uniform particle distribution into a distribution characterized by sharp-edged caustics; note that caustics cannot form for fluid particles, owing to the conservation of phase-plane area associated with the Hamiltonian nature of the system. This constraint does not act for impurites,

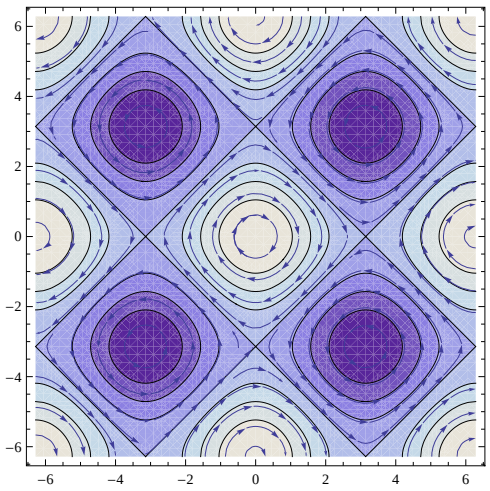

Figure 3: The stationary two-dimensional streamfunction $\psi = 2(\cos x + \cos y)$ and the associated velocity field.

owing to the dissipative nature of the equations describing impurity motion. For light particles, the caustics spiral around the stable fixed points. Hence, for a stationary two dimensional flows, light particles tend to concentrate at the stationary points of the flow; for large enough times the particles are practically absent in the remaining regions of the flow. On the contrary, heavy particles exhibit a very different behavior: After the initial formation of caustics, the heavy particles undergo diffusion along the separatrices of the advecting flow, owing to the chaotic nature of the heavy particle dynamics for the parameter values adopted here.

Figure 5(a) shows the trajectory of an individual heavy impurity in the cellular flow field. The particle alternates between spiralling inward around one of the (now unstable) fixed points and escaping along one of the unstable directions, with a quasiballistic motion. Although this alternance of trapping and quasiballistic motion could be reminiscent of a Lèvy flight, for the system under study the long-time probability distribution of the particle velocity is Gaussian, and it is consistent with a standard Brownian diffusion process.

We can compute the diffusion coefficient for an ensemble of N advected impurities as a function of $\epsilon = 1 - \delta$,

$$D_x = \lim_{t\to\infty} \frac{1}{2tN} \sum_{i=1}^{N} [x_i(t) - x_i(0)]^2 \tag{16}$$

$$D_y = \lim_{t\to\infty} \frac{1}{2tN} \sum_{i=1}^{N} [y_i(t) - y_i(0)]^2 \quad . \tag{17}$$

Figure 5(b) shows the dependence of D_x, D_y on ϵ. Since the flow is isotropic, the two diffusion coefficients are equal. In general, no anomalous (non-Brownian) diffusion has been observed for this system.

In the case of a weakly anisotropic velocity field, one observes some new effects. In the following, we consider the flow described by the streamfunction $\psi = A\cos x + B\cos y$, where $A \neq B$. If one looks at the streamfunction (figure 6), it is evident that there are open "channels" (with our choice of parameters, in the horizontal direction) where the fluid particles undergo ballistic motion. These are analogous to the libration orbits in the phase space of a nonlinear pendulum (the closed orbits would correspond to periodic oscillations). Thus, fluid particles are either trapped inside the cellular regions or undergo ondulating ballistic motion in the channels.

A different story is observed for advected impurities. As for the isotropic flow, light particles sooner or later get trapped at the stagnation points. On the other hand, heavy impurities spend a long time in quasiballistic motion in the channels, and temporary trapping in the cellular regions is followed by jumping off to another channel. Figure 7 shows that an intially uniform particle distribution tends to become spread along the channels, with strong anisotropy.

In this flow, the diffusion coefficients along the x and y directions are very different. Figure 8(b) reveals that D_x, the diffusion coefficient along the channels, diverges with $\epsilon \to 0$, $D_x \sim \epsilon^{-0.6}$ while $D_y \sim \epsilon^{1.5}$. Thus a small anisotropy in the Eulerian flow ($A = 2, B = 2.2$) leads to diffusion coefficients that differ by several orders in magnitude in the case of particles which are only slightly heavier than the fluid ($\delta = 0.9$). This could have interesting consequences for the motion of plankton cells in weakly anisotropic flows, as the small density difference between the plankton cells and the water could result in a strongly anisotropic diffusion of the particles.

5 Neutrally buoyant impurities with finite size

Often, advected impurities have a density that is rather close to that of the fluid (as happens, for example, with most plankton cells), but have a finite size, i.e., they are not fluid elements. To explore the dynamics of these particles, we consider the case of neutrally buoyant particles with $\delta = \rho_f/\rho_p = 1$ and finite, albeit small, radius a. The equation for particle motion in this case becomes:

$$\frac{d\mathbf{V}}{dt} = \frac{D\mathbf{u}}{Dt} - \frac{1}{St}\left(\mathbf{V} - \mathbf{u}\right), \tag{18}$$

where now

$$St = \frac{2}{9}\left(\frac{a}{L}\right)^2 Re, \quad Re = \frac{UL}{\nu}.$$

If we make the approximation that the time derivative along the trajectory of an impurity and that along the trajectory of a fluid parcel are the same, *i.e.* $d/dt = D/Dt$, the problem

becomes very simple. In this case, equation (18) can be written as

$$\frac{d}{dt}\left(\mathbf{V}-\mathbf{u}\right)=-\frac{1}{St}\left(\mathbf{V}-\mathbf{u}\right).$$

Hence

$$\mathbf{V}=\mathbf{u}+\left(\mathbf{V}-\mathbf{u}\right)_0\ \exp\left(-\frac{1}{St}t\right),$$

where $(\mathbf{V}-\mathbf{u})_0$ denotes the initial value of $(\mathbf{V}-\mathbf{u})$. From this we could infer that even if we release a particle with an initial velocity which differs from that of the fluid, after a transient the particle velocity will tend to the fluid velocity, implying that a neutrally buoyant particle will behave, after an initial transient, as an ideal tracer.

In reality, the above conclusion is not correct, as the problem is complicated by the fact that d/dt and D/Dt are not the same. Equation (18) should then be written as

$$\frac{d}{dt}\left(\mathbf{V}-\mathbf{u}\right)=-\left(\mathbf{V}-\mathbf{u}\right)\cdot\nabla\mathbf{u}-\frac{1}{St}\left(\mathbf{V}-\mathbf{u}\right). \tag{19}$$

Defining $\mathbf{M}\equiv\mathbf{V}-\mathbf{u}$, equation (19) can be rewritten as

$$\begin{aligned}\frac{d\mathbf{M}}{dt}&=-\mathbf{M}\cdot\nabla\mathbf{u}-\frac{1}{St}\mathbf{M}\\&=-\left(\mathbf{J}+\frac{1}{St}\mathbf{I}\right)\cdot\mathbf{M},\end{aligned} \tag{20}$$

where $\mathbf{I}$ is the identity matrix and $\mathbf{J}$ is the velocity Jacobian,

$$\mathbf{J}=\begin{pmatrix}\partial_x u & \partial_y u\\ \partial_x v & \partial_y v\end{pmatrix},\quad \mathbf{u}(\mathbf{x})=\begin{pmatrix}u(\mathbf{x})\\ v(\mathbf{x})\end{pmatrix}\ .$$

If we diagonalise the matrix we obtain

$$\frac{d\mathbf{M}_d}{dt}=\begin{pmatrix}\lambda-\frac{1}{St} & 0\\ 0 & -\lambda-\frac{1}{St}\end{pmatrix}\cdot\mathbf{M}_d.$$

From this expression, one can obtain relevant information on the behavior of the advected impurities. For a two-dimensional stationary flow, the difference between the fluid velocity and the particle velocity evolves in time depending on the value of $\pm\lambda-1/St$. In particular, the particle velocity can diverge from the fluid velocity when

$$\lambda^2>\left(\frac{1}{St}\right)^2,$$

from which one sees that the stability of the particle trajectories (with respect to the fluid parcel trajectories) is determined by the balance between the eigenvalues of the fluid velocity field and the Stokes number. When the local value of λ^2 (a property of the Eulerian advecting flow) is sufficiently large, the neutrally buoyant impurity can follow a trajectory that is different from that of a fluid parcel placed at that point.

We can get a further advancement by resorting to the Okubo-Weiss parameter [7, 11]

$$Q \equiv -\text{det}\mathbf{J} = \frac{1}{4}\left(S^2 - \omega^2\right), \tag{21}$$

where $S^2 = (\partial_x u - \partial_y v)^2 + (\partial_y u + \partial_x v)^2$ is the total strain (deformation) and $\omega = \partial v/\partial x - \partial u/\partial y$ is the vorticity. This parameter characterises the local shear/rotational properties of the flow and separates the fluid domain into elliptic and hyperbolic regions [7, 11, 4]:

$$Q \begin{cases} < 0 & \text{rotation} - \text{dominated} \\ > 0 & \text{shear} - \text{dominated.} \end{cases}$$

Since λ satisfies $\det(\mathbf{J} - \lambda\mathbf{I}) = 0$, one has that

$$\lambda^2 - Tr\mathbf{J} + \det\mathbf{J} = 0 \ . \tag{22}$$

In addition, as we are now considering an incompressible flow,

$$\nabla \cdot \mathbf{u} = \partial_x u + \partial_y v = \text{Tr}\mathbf{J} = 0. \tag{23}$$

From (22) and (23), the Okubo-Weiss parameter is then $Q = \lambda^2$. If $Q > 0$, λ is real and deformation dominates, as around hyperbolic points, whereas if $Q < 0$, λ is imaginary and rotation dominates, as in the proximity of elliptic points. Thus, we see that hyperbolic regions can lead to a divergence between the fluid particle paths and the trajectories of the impurities, if they are "hyperbolic enough" (i.e., the value of λ^2 is large enough). As a result, neutrally buoyant impurities will be ejected from hyperbolic regions and will wander around till they end up in elliptic regions, were they will follow the same trajectory of a fluid parcel. This potentially leads to a preferential concentration of neutrally buoyant impurities in elliptic regions, with a biassed sampling of the advecting flow.

5.1 Example 1: Time independent flow

To illustrate the effects of St and Q on the dynamics of a neutrally buoyant particle, we consider the simple incompressible two-dimensional model flow defined by the stream function $\psi(x, y) = A\cos x \cos y$ [1].

Figure 9(a) shows the contour lines of the stream function and of the Okubo-Weiss parameter Q. Figure 9(b) shows the trajectory of a neutrally buoyant particle whose initial velocity is different from that of the fluid at the impurity position. The difference between the velocity of the impurity and the fluid velocity is amplified in highly hyperbolic regions, where impurity trajectories and fluid parcel trajectories separate exponentially. Fig.9(c) shows that the neutrally buoyant impurity has a long and complicated trajectory, wandering between different cells before it comes across the vicinity of an elliptic point and settles in one of the low-Q regions. The time evolution of the difference between the impurity velocity and the fluid velocity at the impurity position is shown in Fig.9(d). Once the impurity has settled in an ellpitic region, the velocity difference between the fluid and the impurity tends to zero an no further instability is observed. However, in their wanderings impurities leave hyperbolic regions, leading to a preferential concentration of neutrally buoyant impurities in the elliptic regions of the flow.

5.2 Example 2: Time periodic flow

The time-dependent flow defined by the stream function $\psi(x, y) = A\cos(x + B\sin\omega t)\cos y$ shows interesting features [1]. As in a typical non-stationary, two-dimensional non-integrable Hamiltonian system, there are regions of phase space where fluid parcels undergo chaotic motion. Figure 10(a) shows the Poincaré section of the chaotic trajectory of a fluid particle, here obtained by plotting the parcel position at times $t = 0, T, 2T, ...$ where $T = 2\pi/\omega$. The trajectory visits a large part of the domain but it is bounded by two separatrices parallel to the x direction, which forbid fluid particle motion across them (remember that the temporal variability is only in the velocity component along x).

The trajectory of a neutrally buoyant impurity, shown in Fig.10(b), indicates that the impurity can wander on a larger portion of the domain, but in the end it converges to a non-chaotic trajectory around an elliptic point. From that moment, the impurity behaves as a fluid particle. However, the impurity has selected a specific sub-domain in space without ever coming back close to its initial conditions, at variance with what would have happened for a Hamiltonian system. The equations of motion for a neutrally buoyant impurity are dissipative, and there is no conservation of phase-space volume. For completeness, Fig.10(c) shows the difference between the velocity of the impurity and that of the fluid, as a function of time.

5.3 An application to two-dimensional turbulence

The results discussed above have interesting implications for two-dimensional turbulent flows [1, 9]. We integrate the two-dimensional vorticity equation for an incompressible fluid with bi-harmonic (hyper)viscosity,

$$\frac{\partial\omega}{\partial t} + J(\psi, \omega) = -\nu_h \nabla^4 \omega, \tag{24}$$

where ψ is the stream function, $\omega = \nabla^2\psi$ is the vorticity, $u = -\partial_y\psi$ and $v = \partial_x\psi$ are the velocity components and the hyperviscosity parameter is $\nu_h = 2.5 \times 10^{-7}$. To integrate the equation, we use a pseudo-spectral method with 512^2 collocation points in a doubly periodic domain; here we consider a freely-decaying case with no external forcing. In this flow, an initially homogeneous distribution of neutrally buoyant impurities evolves in time towards a distribution where the impurities are concentrated in the inner part of vortices, where $Q < 0$, as shown in Fig.11. This may have interesting consequences when we design fluid experiments using neutrally buoyant tracer particles, as one should verify that the tracers really provide an unbiassed sampling of the velocity field.

6 The role of rotation

The presence of a rotation introduces new effects in the dynamics of the heavy impurities [9]. When the (apparent) Coriolis and centrifugal forces are acting on an impurity, the dimensional equation for the impurity motion becomes

$$\frac{d\mathbf{V}}{dt} = \delta\frac{D\mathbf{u}}{Dt} - \frac{1}{\tau_a}(\mathbf{V} - \mathbf{u}) - (1 - \delta)\, g\hat{\mathbf{z}} - 2\boldsymbol{\Omega} \times (\mathbf{V} - \delta\mathbf{u}) + |\boldsymbol{\Omega}|^2 \mathbf{R}\,(1 - \delta)\,, \tag{25}$$

where δ and τ_a are defined as before and $\mathbf{R}$ is the distance of the particle from the axis of rotation. Notice that the term $-2\delta\mathbf{\Omega}\times\mathbf{u}$ had to be subtracted from the Coriolis term acting on the impurity because it was already taken into account in the expression $\delta D\mathbf{u}/Dt$. Thus, the Coriolis term acts on the density-weighted difference between the velocity of the impurity and that of the fluid. Non-dimensionalising the above equation, we obtain

$$\frac{d\mathbf{V}}{dt}=\delta\frac{D\mathbf{u}}{Dt}-\frac{1}{St}\left(\mathbf{V}-\mathbf{u}\right)-\left(1-\delta\right)\tilde{g}\hat{\mathbf{z}}-\frac{1}{R_o}\hat{\mathbf{z}}\times\left(\mathbf{V}-\delta\mathbf{u}\right)+\frac{1}{4R_o}\frac{\mathbf{R}}{L}\left(1-\delta\right), \tag{26}$$

where St is defined as before and

$$Ro=\frac{U}{2\Omega L}$$

is the Rossby number. Fig.12 shows a distribution of 8000 heavy impurities which were initially homogeneously distributed in a statistically stationary numerical simulation of forced and dissipated 2D turbulence [9]. The numerical integration has been performed in the doubly periodic domain $[0,2\pi]\times[0,2\pi]$ with 128×128 collocation points. The particles have $\delta=0.8, St=0.01$ and $Ro=1/320$. In the integration, we have discarded the effect of the centrifugal force. The heavy impurities concentrate inside the centers of the anticyclonic vortices, leaving both the turbulent background and the cores of cyclonic vortices. This is due to the fact that the Coliolis force adds up to the inertial force to eject heavy impurities from cyclones, whereas it works against the inertia to push impurities towards the center of anticyclones. When Ro is small enough, the Coriolis force overcomes the centrifugal effect of inertia and the impurities concentrate in the cores of anticyclonic vortices. When the vortices are especially intense, they generate a strong centrifugal force due to the particle inertia. The strength of the centrifugal push by the vortex becomes weaker when the distance from the vortex center increases. In this case, the Coriolis force balances inertia at some distance from the vortex center and the impurities concentrate in an annular distribution inside the vortex.

As a final example, we momentarily leave the world of plankton and discuss the (again idealized!) motion of dust grains in the solar nebula [2]. In this case, $\delta\sim10^{-8}$ so that we may may discard the term $\delta\, D\mathbf{V}/Dt$. The impurity equation is then reduced to

$$\frac{d\mathbf{V}}{dt}=-\frac{1}{\tau_a}\left(\mathbf{V}-\mathbf{u}\right)-\nabla\Phi-2\mathbf{\Omega}\times\mathbf{V}+\left|\mathbf{\Omega}\right|^2\mathbf{R}, \tag{27}$$

where Φ is a gravitational potential. In the specific case of particles spinning around the protosun in the solar nebula (a rarefied fluid composed mainly by hydrogen) the equation of motion of a dust particle becomes

$$\frac{d\mathbf{V}}{dt}=-\frac{1}{\tau_E}\left(\mathbf{V}-\mathbf{u}\right)-2\mathbf{\Omega}\times\mathbf{V}-\frac{GM}{R^2}\hat{\mathbf{R}}+\left|\mathbf{\Omega}\right|^2\mathbf{R}. \tag{28}$$

Here, G and M are the gravitational constant and the mass of the protosun, respectively. For the rarefied conditions of the protoplanetary nebula, the friction time scale τ_E is set to have the form $\tau_E\propto a/\rho_f$, where a is the radius of the particle. This expression of the drag

coefficient corresponds to what is called the Epstein regime for a rarefied gas.

To proceed with the study, we consider a simplified representation of the protosolar nebula by using a two-dimensional turbulent flow subject to a circularly-symmetric Keplerian shear, physically generated by the presence of a central massive object (the protosun) [2]. Figure 13(a) shows the vorticity field at sufficiently large time, obtained by numerical simulation of this system. By perturbing the initial Keplerian shear (which is linearly stable in the absence of magnetic effects), both cyclonic and anticyclonic vortical perturbations tend to form. However, cyclonic vortices are rapidly destroyed by the adverse shear - or do not form at all - and only anticyclonic vortices survive in the Keplerian shear, as illustrated in Figure13(a). As already seen in the case of standard two-dimensional turbulence discussed above, the heavy impurities tend to concentrate inside the anticyclonic vortices as time progresses. Fig.13(b) shows the distribution of an ensemble of heavy impurities, initially released with a uniform distribution, in the flow field of Fig.13(a). From these results, one could speculate that dust grains in the solar nebula could be concentrated by the dynamics in the cores of anticyclonic vortices, where the subsequent evolution (collisions, gravitational attraction) could more easily ensue.

7 Conclusion

The dynamics of passively advected impurities is quite different from that of fluid parcels. From a mathematical point of view, the phase space of the impurity motion has twice the number of dimensions of that of the fluid parcels, since it is described by particle positions and velocities instead of just particle positions, as in the case of fluid elements. In addition, the presence of Stokes drag makes the system dissipative, with the possibility of non-homogeneous particle distributions in space and preferential particle concentrations in specific regions of the flow. Physically, this means that advected impurities may provide a non-homogeneous sampling of the fluid domain. Even neutrally buoyant impurities, when their size is large enough, can behave very differently from fluid parcels. All these results indicate that small objects immersed in a fluid - such as plankton cells in water or dust grains in the solar nebula - can undergo complicated dynamics which cannot be understood only from considering the motion of fluid particles.

Before closing this lecture, it is important to recall that so far we have simplified the description, neglecting for example the effect of unsteady forces associated with the acceleration of the impurities, such as the added mass term [6] and the Basset force [10]. These two terms become important especially when $\delta = \rho_f/\rho_p \sim 1$. Full consideration of the Basset term is especially important, but difficult from a numerical point of view owing to the need of storing the past trajectories of a large number of particles. Further complications arise from considering non-spherical particles, a fact which induces new effects, see for example [8] for experimental results on the dynamics of sinking particles with plankton-like shapes and [5] for a theoretical study of the dynamics of elongated impurities.

References

[1] Babiano, A., J. H. E. Cartwright, O. Piro, and A. Provenzale, "Dynamics of a Small Neutrally Buoyant Sphere in a Fluid and Targeting in Hamiltonian Systems", *Phys. Rev. Lett.*, **84**, 5764–5767 (2000).

[2] Bracco, A., P. H. Chavanis, A. Provenzale, and E. A. Spiegel, "Particle aggregation in a turbulent Keplerian flow", *Phys. Fluids*, **11**, 2280–2287 (1999).

[3] Crisanti, A., M. Falcioni, A. Provenzale, P. Tanga and A. Vulpiani, "Dynamics of passively advected impurities in simple two-dimensional flow models", *Phys. Fluids A*, **4**, 1805–1820 (1992).

[4] Koh, T-Y. and B. Legras, "Hyperbolic lines and the stratospheric polar vortex", *Chaos*, **12**, 382–394 (2002).

[5] Mallier, R. and M.R. Maxey, "The settling of nonspherical particles in a cellular flow field", *Phys. Fluids A*, **3**, 1481-1494 (1991).

[6] Maxey, M. R. and J. J. Riley, "Equation of motion for a small rigid sphere in nonuniform flow", *Phys. Fluids*, **26**, 883-889 (1983).

[7] Okubo, A. "Horizontal dispersion of floatable particles in the vicinity of velocity singularities such as convergences", *Deep-Sea Res.*, **17**, 445–454 (1970).

[8] Padisák, J., E. Soróczki-Pintér and Z. Rezner, "Sinking properties of some phytoplankton shapes and the relation of form resistance to morphological diversity of plankton an experimental study", *Hydrobiologia*, **500**, 243-257 (2003).

[9] Provenzale, A., "Transport by coherent barotropic vortices", *Annu. Rev. Fluid Mech.*, **31**, 55–93, (1999).

[10] Reeks, M. W. and S. Mackee, "The dispersive effects of Basset history forces on particle motion in a turbulent flow",*Phys. Fluids*, **27**, 1573–1582 (1984).

[11] Weiss, J. "The dynamics of enstrophy transfer in two-dimensional hydrodynamics", *Physica D*, **48**, 273–294 (1991).

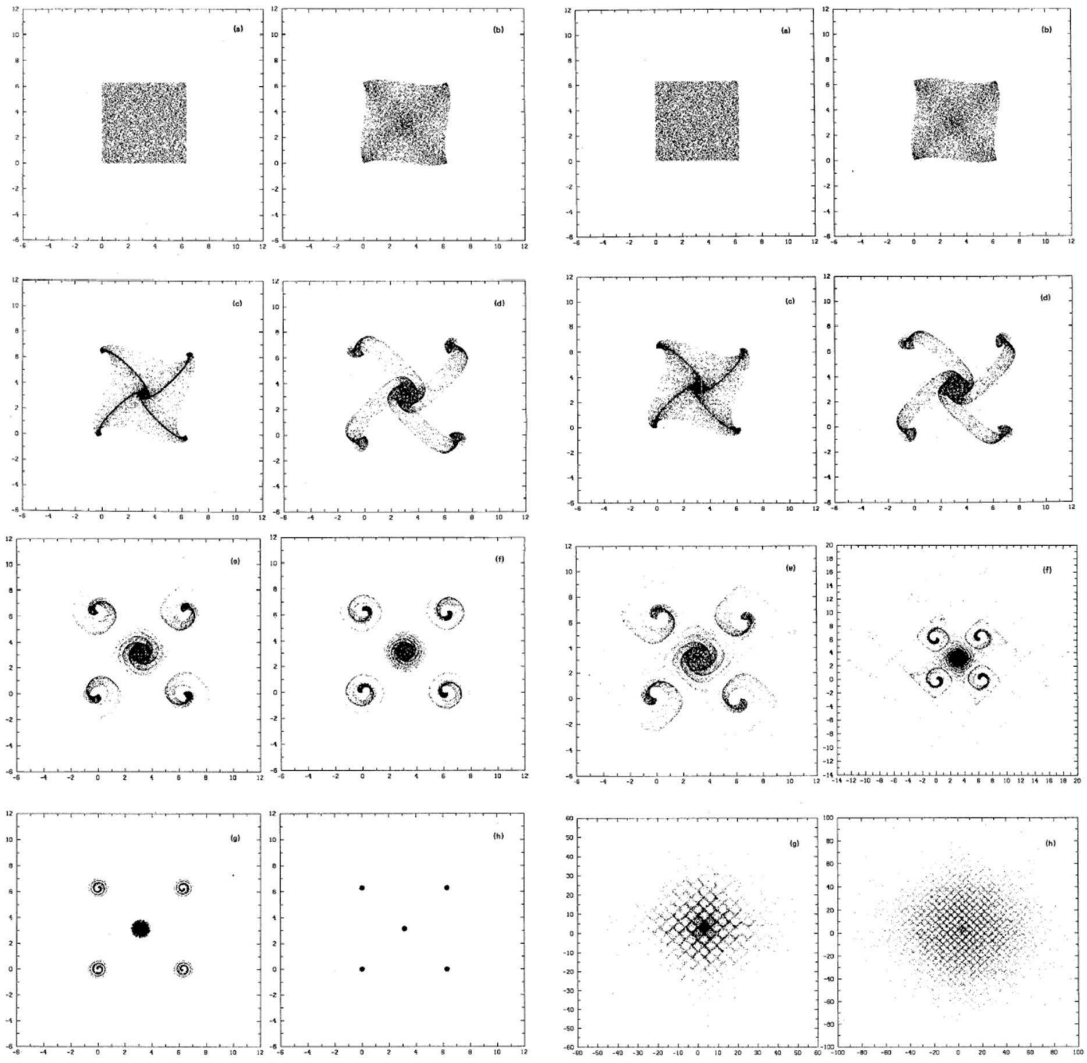

(a) $\delta = 1.1$ (b) $\delta = 0.9$

Figure 4: Distribution of 10,000 impurities with density ratio $\delta = 1.1$ (left panels) and $\delta = 0.9$ (right panels) and $St = 1$ in the advecting flow defined by the stream function $\psi = 2(\cos x + \cos y)$. The individual panels refer to different times, namely $t = 0, 0.5, 1, 2, 5, 10, 40$ and 100 non-dimensional time units.

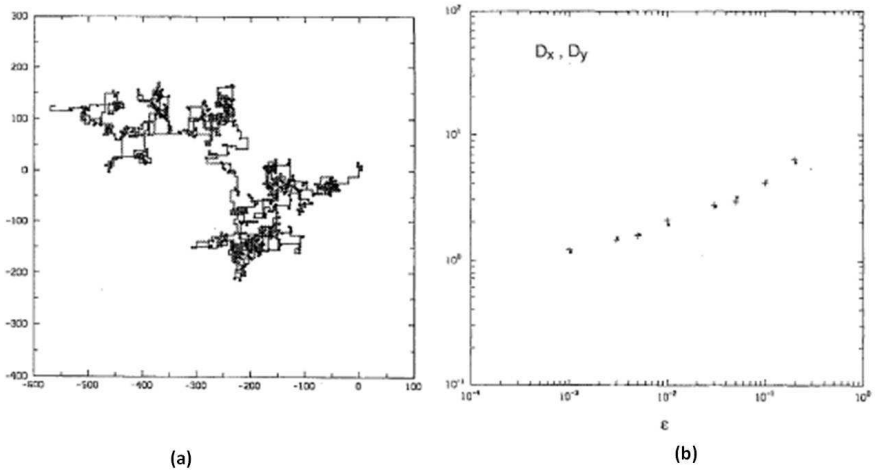

Figure 5: (a) Trajectory of an individual advected impurity with density ratio $\delta = 0.9$ and $St = 1$ in the flow defined by $\psi = 2(\cos x + \cos y)$, from $t = 0$ to $t = 10000$ non-dimensional time units. (b) Diffusion coefficients along x and y, D_x (stars) and D_y (crosses), for an ensemble of heavy impurities as a function of $\epsilon = 1 - \delta$.

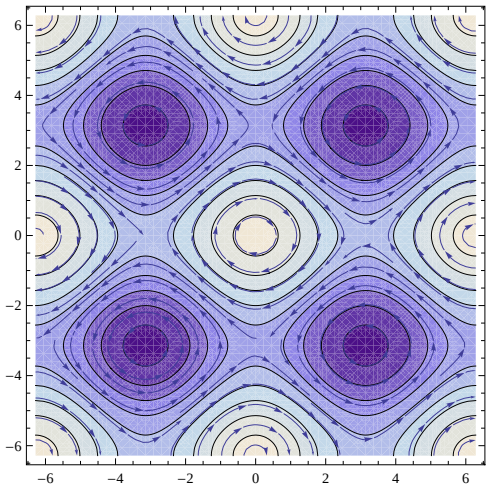

Figure 6: Streamfunction and the corresponding velocity field for the anisotropic cellular flow described by $\psi = (A \cos x + B \cos y)$ with $A = 2$ and $B = 2.4$.

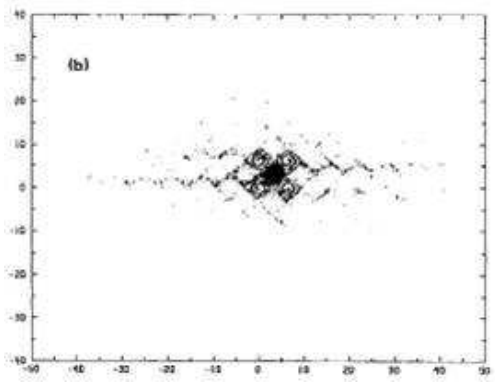

Figure 7: Distribution of 10,000 impurities of density ratio $\delta = 0.9$ and $St = 1$ in the Eulerian flow defined by the anisotropic stream function $\psi = (A\cos x + B\cos y)$. $A = 2$, $B = 2.4$.

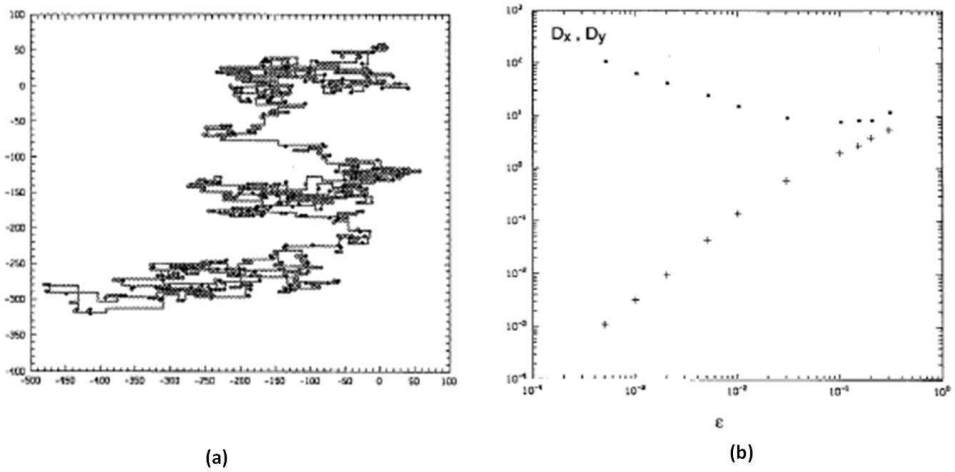

Figure 8: (a) Trajectory of an individual advected impurity with density ratio $\delta = 0.9$ and $St = 1$ in the Eulerian flow defined by the anisotropic stream function $\psi = (A\cos x + B\cos y)$ with $A = 2$ and $B = 2.4$, from $t = 0$ to $t = 10000$ natural time units. (b) Diffusion coefficients, D_x (stars) and D_y (crosses), for heavy impurities as a function of $\epsilon = 1 - \delta$, for $A = 2$ and $B = 2.2$.

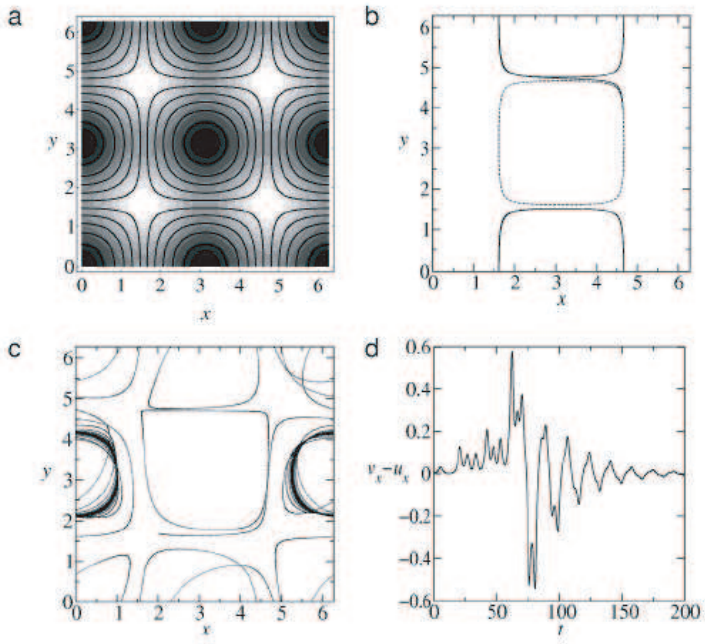

Figure 9: (a) Fluid parcel trajectories (thick lines) and magnitude of the Okubo-Weiss parameter Q (background shading, lighter shading correspond to positive values of Q), for the stream function $\psi = A \cos x \cos y$. (b) Trajectory of a neutrally buoyant impurity with Stokes number $St = 0.2$ (solid line) and path of a fluid particle starting at the same initial position of the impurity (dashed line). The instability in regions of high Q allows the impurity to wander between cells, diverging from the streamlines. (c) After a complicated excursion, the neutrally buoyant impurity eventually settles in a zone of low Q. (d) Difference between the velocity of the impurity and the fluid velocity at the instantaneous impurity position.

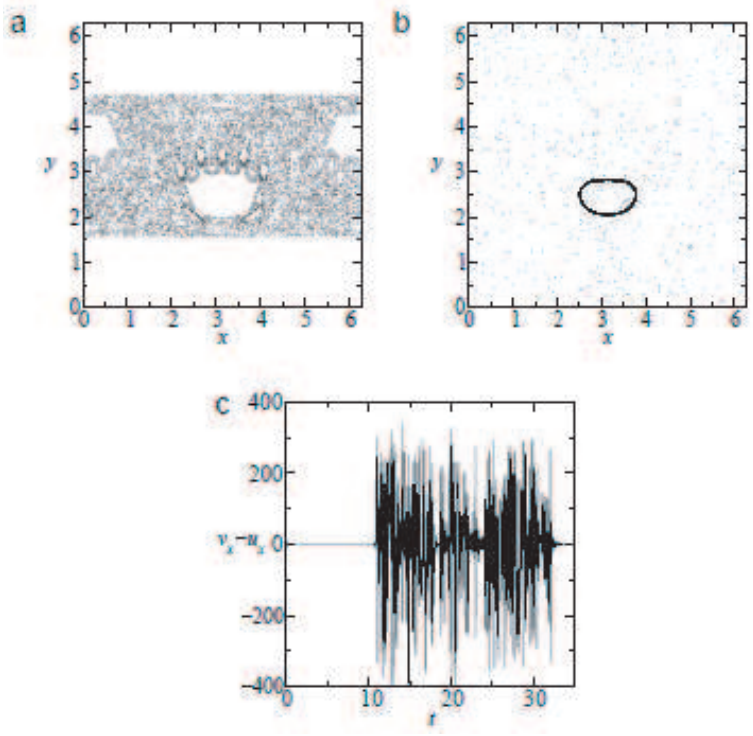

Figure 10: The upper panels show the Poincaré sections of a fluid parcel trajectory (a) and of a neutrally buoyant impurity with $St = 0.2$ (b) in a time-dependent cellular flow with $A = 250, B = 0.3$, and $\omega = 1.0$. Panel (c) shows the time series of the difference between the velocity of the impurity and the fluid velocity at the impurity position.

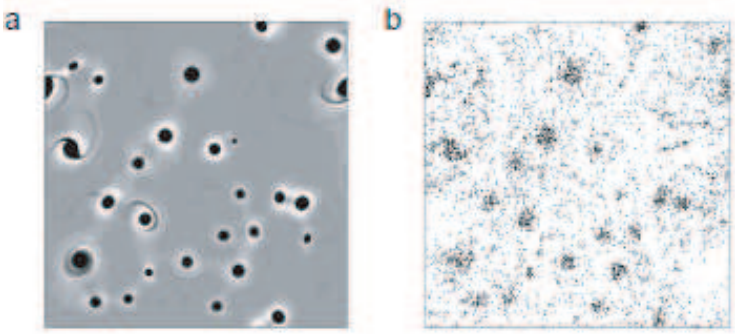

Figure 11: Small neutrally buoyant impurities with Stokes number $St = 0.2$ tend to concentrate in the centers of vortices in a two-dimensional turbulent flow. Panel (a) shows the distribution of the Okubo-Weiss parameter Q at time $t = 1$ non-dimensional units (lighter shading corresponds to larger Q, that is, to hyperbolic regions). Panel (b) shows the distribution of neutrally buoyant impurities which were initially uniformly distributed in the flow domain.

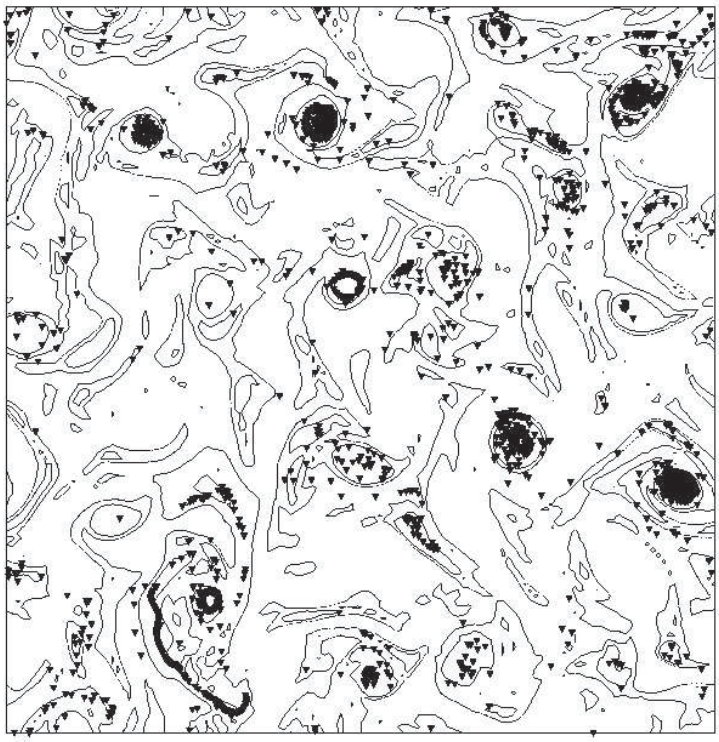

Figure 12: Distribution at $t = 6$ non-dimensional time units of 8000 heavy impurities advected by forced, statistically stationary two-dimensional turbulence in a cyclonically rotating reference frame. Small solid triangles indicate the positions of the advected particles and thin solid curves indicate vorticity isolines. The impurities concentrate in the cores of anticyclonic vortices. Parameter values are $\delta = 0.8, St = 0.01$, and $Ro = 1/320$.

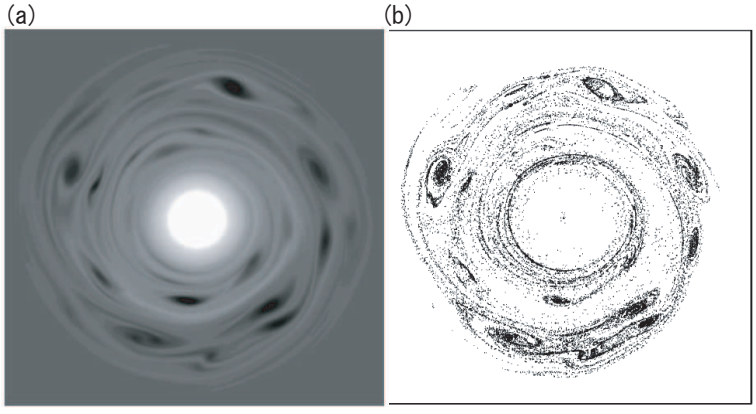

Figure 13: Panel (a) shows the vorticity field at $t = 15$ non-dimensional time units for our idealization of the flow in a protosolar nebula. Panel (b) shows the distribution of heavy impurities at the same time.